Chapter 3

Wear and Corrosion Behavior in Different Materials

N. A. de Sánchez, H. E. Jaramillo, H. Riascos,
G. Terán, C. Tovar, G. Bejarano G., B. E. Villamil,
J. Portocarrero, G. Zambrano and P. Prieto

Additional information is available at the end of the chapter

http://dx.doi.org/10.5772/52986

1. Introduction

This chapter presents three articles with results, about our research, relationships with the behavior corrosion resistant in different materials of engineer. The first research is about TiC monolayers and Ti/TiN/TiC/TiCN multilayers were deposited onto AISI 4340 steel substrates at 300º C and $4.0x10^{-2}$ mbar nitrogen/methane pressures by using a Pulsed-Laser Deposition technique. A Nd: YAG laser (1064 nm, 500 mJ and 7 ns), with a repetition rate of 10 Hz was used. Here we analyzed the difference in structure and morphology for single layers and multilayers structures deposited on stainless steel substrates. AFM analysis presented different morphologies; showing, that the single layer had an average grain size of 0.087 μm; while the multilayers exhibited grain sizes of 0.045 μm. Coating thicknesses were 1 μm, approximately, and monolayer average roughness was 0.21 μm; while a value of 0.15 μm was measured for multilayers. Under a 60 Kg maximum load applied in tension to evaluate the adhesion to the substrate, no detachment of the films was presented. Multilayers evidenced better impact resistance as compared with TiC single layer; this result is considered, bearing in mind that in multilayers propagation of fissures is slower, because the presence of layer inter-phases, lead to fissures strays in other directions. Slight corrosion specks are present; but mass loss was around 16 mg. in multilayers a value was lower than for the TiC single layer that was near 43 mg. Homogeneity, grain size, fracture resistance, corrosion resistance, and adhesion of the multilayers are suitable for mechanical applications of these types of coatings as shown in mechanical measurements. These results indicate that for engineering applications under corrosive environments, the use of this type of multilayers coatings on AISI 4340 steel, are highly recommended.

In the second research we present results of corrosion test analysis on 304-type stainless steel welded samples. The samples were welded by SMAW, GMAW, and GTAW techniques. Corrosion tests were carried out under normal working conditions. The samples were installed on the ventilation extractor at a sugar mill, with a pull inducement to facilitate the rise of gases containing concentrations of smoke and sulfur and sulfide vapors, which generate a low PH within the tower. The samples were removed from the ventilator vents at 15-day programmed intervals, until completing 16 samples, for the purpose of studying the advancement of corrosion dependent of exposition time. Filler welt morphologies were analyzed by using Scanning Electron Microscopy SEM; the interface between the filler metal and base metal was studied by means of an image analyzer. SEM microscopy revealed that samples treated with the GMAW welding process presented the phenomenon of segregation upon the solder welt. Through EDX analysis we found the formation of carbides, which explains the presence of the segregation phenomenon. Due to the loss of chromium at the solder welt, there was the generation of a greater corrosion zone in these simples treated with GMAW processes compared to simples treated with SMAW and GTAW welding techniques. The migration of carbon to zones of greater segregation favored the carbide formation, which cause diminished corrosion resistance. Additionally, given the chemical dissimilarity between the segregated and non-segregated zones, a galvanic pair was generated that increased the phenomenon.

And the final we show WC/W coatings were deposited by reactive magnetron sputtering using 40%, 60% and 80% methane CH4 in the gas mixture. The bilayers were grown on to AISI 420 stainless-steel substrates in order to study the wear and corrosion behavior. Before growing the bilayers, one Ti monolayer was grown to improve the adherence of the coatings to the substrate. The wear resistance and the friction coefficient of the coatings were determined using a pin-on-disk tribometer. All coatings had a friction coefficient of about 0.5. The measured weight lost of the bilayers from each probe allowed the qualitative analysis of wear behavior all coatings. The bilayers grown with 80% methane showed the best abrasive wear resistance and adhesion without failure through the coating in the wear track for dry pin-on-disk sliding. Electrochemical corrosion test showed that the bilayers grown with 80% methane were more resistant to corrosion than the ones uncoated.

2. Preface

The need to improve the physical/mechanical properties of materials has led to the development of new hard and super hard coatings with hardness over 40 GPa as compared with the hardness of diamonds, (96±5 GPa) [1]. Some examples of these coatings are: Carbon Nitrate [2,3,4], Nitrate super networks [5], and Oxide super networks [6], and high wear resistance [7].

Hard coatings that are mostly resistant to wear and corrosion have been commercially utilized to increase the useful life of a number of industrial elements, such as: cutting tools, gears, bearings, and industrial machinery components [8]. Applications include protection coat-

http://dx.doi.org/10.5772/52986

ings, thermal barriers, optical applications, bio-medicine, semiconductors, and decorative uses. In the last decades, intensive work has been carried out on hard coatings by different research groups. With hard coatings it is possible to improve the surface properties of materials or those properties that are dependent of the surface, as are: hardness; corrosion, fatigue, and wear resistance. [8] These properties, together with the electrical, magnetic, and optical properties are not only of scientific interest, but also of technological interest, being that in both mechanical and biological systems it is necessary to improve the useful life of elements; save energy; and improve their efficiency and reliability.

Metallic materials, especially steel, upon which hard coatings are applied, present high surface hardness, low friction coefficient, high resistance to wear, high resistance to fatigue and corrosion, and dimensional stability at working temperatures bellow 500 °C [4]. The aforementioned characteristics are dependent of several factors, like the type of material to be coated, the kind of coating, and compatibility and adhesion of the hard coating upon the material to be coated. In the specific case of pulsed-laser ablation technique, certain parameters should be observed; such as: the chamber's vacuum pressure, pulse duration, rate of repetition, temperature of the substrate, gas ratio. In film growth we must bear in mind the crystalline structure, the film's homogeneity, density, thickness, and its chemical and morphological composition.

Recently, there has been a great deal of attention to the production of multilayers, mainly multilayers of ceramic/ceramic transition metal nitrates, each of the layers in the scale of nanometers, due to the possibility of obtaining super hardness [9,10,11]. There is improvement in the tribologic properties of metal/metal nitrates or in the multilayers of oxides; this area has attracted the interest of research groups [12]. In recent studies, J.P. Tu et al, [13]. analyzed Ti/TiN multilayers with a soft compositional transition, which they produced with computer-controlled gas flow. The results revealed that both the interfaces, as well as the period modulation of the multilayers play an important role in improving mechanical properties [14,15]. This work compares the structure, morphology, grain size, fracture resistance, wear resistance, and corrosion resistance of multilayers as opposed to monolayers.

In industrial processes, one of the most widely used materials is stainless steel, given its excellent anticorrosion, mechanical, and aesthetic properties. But when stainless steel is attacked by acidic agents under certain concentration parameters, its behavior as an anticorrosive material may not be the best; and steel can be attacked with great severity.

Corrosion is defined as the deterioration of material as a result of chemical attacks within its environment [20]; corrosion refers specifically to any process involving the deterioration or degradation of metal components [21]. More specifically, it can be defined as a chemical or electrochemical reaction between a material – normally a metal – and its environment, producing deterioration of the material and its properties [22]. As much as corrosion is originated from a chemical reaction, the velocity at which it will take place will depend, in some measure, on temperature, salinity of the fluid, and properties of metals in question [23].

Different types of corrosion can appear on stainless steel, depending on the aggressor medium and surface conditions, roughness, chipping and residual efforts. The types of corrosion that can appear are inter-granular corrosion, corrosion by chipping, corrosion by efforts, galvanic corrosion [24] etc. Bearing in mind the aforementioned, we present the study of deterioration of austenitic 304 stainless steel joined through welding with SMAW, GTAW, and GMAW [25] processes and exposed to an industrial environment, namely, the sulfitation tower in a sugar mill, subjected to sulfur gases.

It is well established that the mechanical, tribological and thermal properties of many metals can be significantly improved by the controlled incorporation of interstitial elements, such as boron, nitrogen and carbon. Although W and WC coatings have been used for a number of applications [31], there seems to be a lack of knowledge about coatings with carbon concentrations [32] at the intermediate range below that of stoichiometric WC. Tungsten carbide, silicon carbide and silicon nitride are predicted to be among the most abrasion-resistant tool materials [33] and are known to be effective in resisting erosion [34]. Dimigen and co-workers developed tungsten metal doped DLC (W:C-H) coatings with W/C ratios of around 0.1 [35,36].These have attracted considerable attention, owing to their high wear resistance and low friction coefficient.

One of the major drawbacks of the wear tests is the scarce reproducibility of the experimental data. In citing the results of a UK inter-laboratory project of a single pin-on-disk test on wear-resistant steels worn under fixed test conditions, Almond and Gee [37] reported dispersion in the range of 57.2–75.4% for the wear data and a minimum reproducibility of 37% for the friction coefficient. Considering the repeatability within laboratories, the latter value was in the range of 3–19%. These great dispersions, especially for the wear data, were mainly attributed to the difficulty of properly mating the flat-end pin surface with the disk surface in the different test machines of the laboratories involved in the project.

3. Experimental details mechanical behavior of TiC monolayers and Ti/TiN/TiC/TiCN multilayers on AISI 4340 steel

TiC monolayers and the multilayers analyzed in this work were grown on AISI 4340 steel through the laser ablation technique. An INDI-30 spectra-Physics TM Q-switched Nd: YAG pulsed laser was used with energy at 500 mJ, pulse duration of 7 ns, a wavelength of 1064 nm, and a repetition rate of 10 Hz. The TiC films were grown from a high-purity Ti target in the order of 99.999% in an atmosphere of Ar, N_2, and CH_4 gases. The coatings were grown at a temperature of 300 °C; pressure of 4.0×10^{-2} mbar was kept constant during the growth of all films. The thickness of the films was approximately 1 μm.

The films were characterized by Atomic Force Microscopy (AFM), Electronic Scaning Microscopy (SEM), resistance to wear, resistance to fracture, and resistance to corrosion. This

work analyzed the difference in structure and morphology of the monolayers and multilayers deposited upon a similar type of substrate.

The adherence of the films grown on steel substrates was estimated by way of tests, using normalized Y-type adhesive tape of L-T-90[1] specifications according to procedures described in norm MIL – F – 48616 [2]. For such, the tape was firmly applied over the film, without reaching the borders to keep from tearing the films at inhomogeneous regions that could be present on the contour and, thereby, avoiding the formation of air bubbles. Thereafter, while the substrate was being held with tweezers, the tape was quickly removed at a normal angle to the film surface. All monolayers and multilayers analyzed passed the test with no apparent visual deterioration, thus indicating that the adherence to the substrate is acceptable.

Also, adhesion tests of the films were carried out through the application of tension loads. The substrate with the film was placed over a test tube used for the tension trial. The sample was adhered with Loctite 495 glue, superdner instant adhesive.

Progressive loads were applied 5Kg at a time till reaching 60Kg. Upon applying the maximum 60Kg load, the substrate with the film separated from the glue, but the film did not reveal any detachment after the visual check, with which it is concluded that the adherence of the films is acceptable and superior to the capacity of the glue's adhesion.

The TiC films and the multilayers were exposed to a wear test by using a G99 pin on disc type tribometer. The pin corresponded to the analyzed film and the AISI D2 steel disc with a roughness of 0.71μm. was worked with a velocity of 0.1 m/s. A 30 gr. load was applied for 5 min. The prior conditions remained constant during the analysis of all the films.

The film's resistance to fracture was assessed using the Rockwell C hardness test. As of the analysis of traces left by the indenter, it was found that the multilayers are more resistant to fracture than the TiC monolayers. Adhesion of the films was determined by the tension test; maximum loads of 60 Kg were applied and neither the monolayers nor the multilayers showed signs of substrate detachment.

The monolayers and multilayers were exposed to corrosion-erosion tests, using the equipment shown in figure 1. The specimen were impingement with a slurry composed by a 0.2 pH solution with 30 wt.% of SiO_2 particles with mean size between 212 and 300 μm. The impeller device was a UHMWPE disk at 3500 rpm rotation speed. The surface impact area was 0.05 m^2; the slurry temperature varied between 25 and 28 °C and the test time were one (1) hour.

The mean impact angle was 30 °C but it is worth to notice that the dispersion is great due to several factors as boundary layers and viscosity effects, that deviate the particles as they are reaching the probes surfaces [18].

1 Tape As Per MIL-A_AA-113B

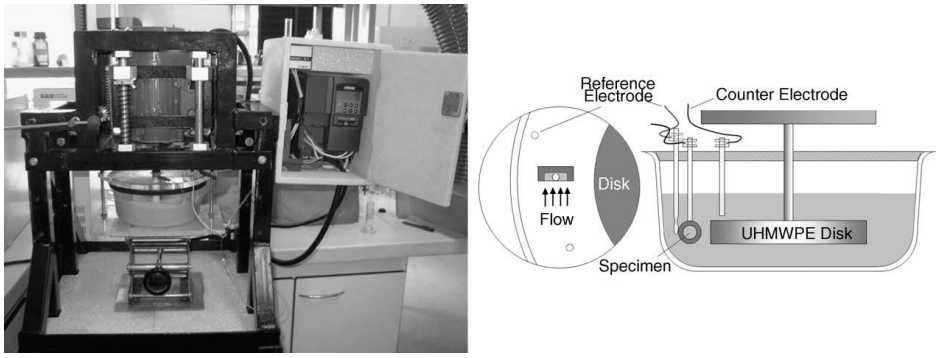

Figure 1. Experimental setup for liquid impingement and corrosion–erosion tests.

4. Results and analysis

All the films underwent AFM analysis to determine the morphology and structure as a function of the substrate. AFM images in figure 2 show the TiC film and the multilayer, revealing, in both cases, high-homogeneity surfaces free of pinholes or agglomerates. The multilayer has very fine and uniform grain size, while the TiC monolayer surface shows somewhat larger grain size and a less homogenous distribution.

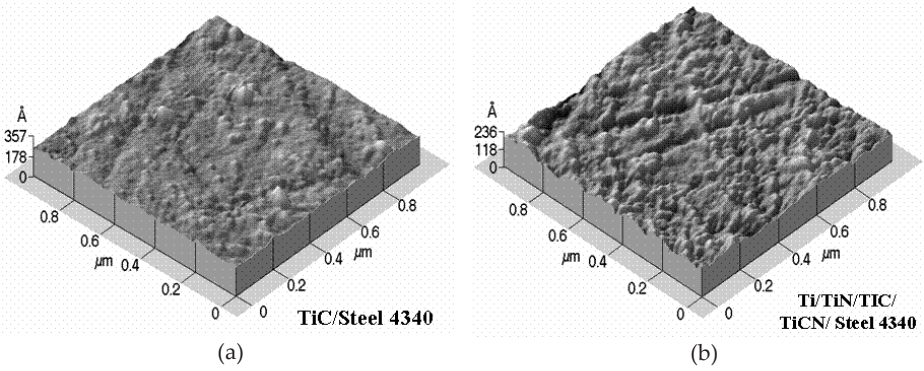

Figure 2. AFM Micrographs of a) TiC and b) multilayers grown on AISI4340 steel.

Two-dimensional AFM micrographs in figure 3 show the differences in grain size for the monolayers and the multilayers: the monolayers had an average grain size of 0.087 μm, while the multilayers exhibited grain sizes of 0.045 μm. Roughness for the monolayers was at 0.21 μm, and for the multilayers it was at 0.15 μm.

http://dx.doi.org/10.5772/52986

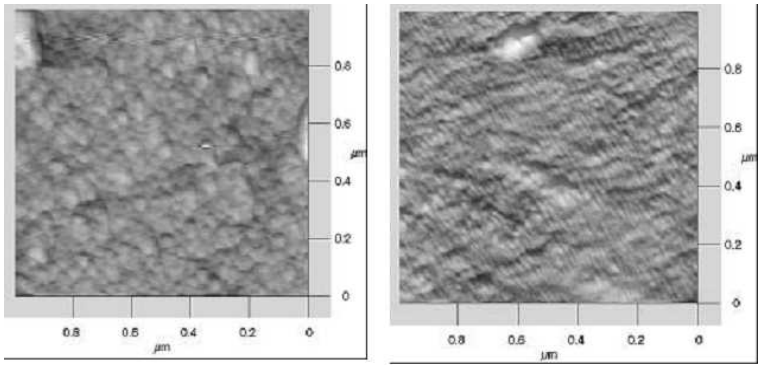

Figure 3. AFM Micrographs of a) TiC monolayers and of b) Multilayers, where the grain- size difference is observed.

Monolayers and multilayers were exposed to a wear test by using a G99 pin on disc type tribometer. The micrograph of the TiC film in figure 4a shows where there was the most wear on the film; the wear produced was of 0.0008 gr., while the multilayer did not reveal wear at the end of the test according figure 4b.

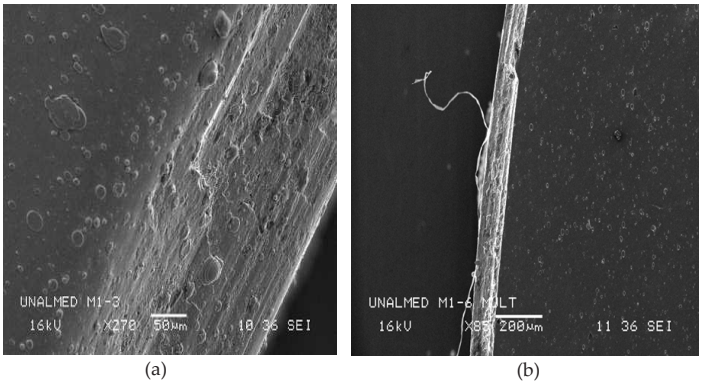

Figure 4. SEM Micrographs after wear test: a) TiC monolayer, b) multilayer.

The coatings were characterized through the Rockwell C hardness test to qualitatively determine their resistance to fracture. Loads of 60 Kg, 100 Kg, and 150 Kg were applied to the monolayers and the multilayers. Optical photographs were taken of the traces left by the indenter upon the application of the three different loads. Figure 5a shows traces left by the indentations carried out upon the TiC coatings at different loads. Upon observation of microscopic images, radial fractures are detected toward the interior – keeping the radial directionality and without notable detachment of the film.

The micrographs in figure 5b correspond to Rockwell C indentations applied to the multilayers. It was microscopically observed that the plastic deformation around the trace is very slight and that the film did not suffer any detachment. When load is increased, densities of the fissures around the trace diminish in density.

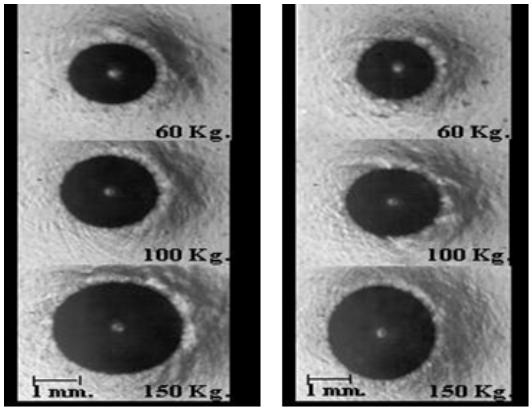

(a) (b)

Figure 5. Images of Rockwell C indentation traces a) upon TiC monolayers, and b) on multilayers, (charges are indicated).

The generation of circumference fissures observed is due to radial tension efforts outside of the indentation zone. As the load is increased, these are submitted to compression efforts. The propagation of fissures with a load of 60 Kg. curve and run parallel to the surface, such is explained by a field of compressive tensions according to Bhowmicks et all [19]. The multilayers showed better impact resistance as compared with the TiC monolayers. This result is considered, bearing in mind that in the multilayers the propagation of fissures is slower, because on the interphase of the coatings the fissures stray in another direction.

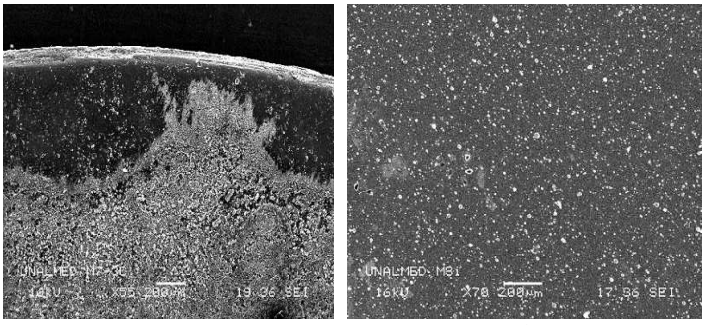

(a) (b)

Figure 6. SEM Micrographs after corrosion test in a saline atmosphere a) TiC film b) multilayer.

As can be seen in figures. 6a and 6b corresponding to SEM micrograph of TiC and multilayer coatings respectively. The TiC films were severe worm out while on the multilayers we observed formation of pits. The TiC mass lost was 0.043 g and the multilayers´ one was 0.016. g. We observed that the monolayers were more vulnerable to corrosion - erosion test.

5. Experimental details corrosion effects on SMAW, GMAW, and GTAW welding processes stainless steel 304

In the development of the welding process, GMAW, GTAW, and SMAW techniques were used with welding equipment. The first arc welding process was applied following international welding norms, using austenitic 304 stainless steel plates [26] with dimensions of 50 x 20 x 4.76 mm. A coated electrode series E308L-16 was used. The time of application of the welding chord was of 1'57"64'", with power at 38V and current at 85A. The same characteristics, variables and equal working conditions were used for GTAW and GMAW welding processes.

The corrosion test, to which the samples were subjected, is classified as a field test [22] With this test we seek to determine which is the Contributing Metal and Base Metal in the Thermally Affected Zone that is least affected by the aggressive medium, that fundamentally is acidic type like smoke emissions and sulfur vapors, as well as its relationship with the welding process used.

The experimental phase was carried out at a sugar mill, since this type of industry is one of the most affected by corrosion problems. It was determined that the most severe corrosive medium and the highest corrosion levels in the sugar mill for the tests took place in the sulfitation towers, where there are elevated concentrations of sulfur and sulfides smokes and vapors, which generate low PH [27] which is an ideal environment for the study of corrosion in the Contributing Metal and Base Metal in the Thermally Affected Zone, in 300-series stainless steels like the 304.

The samples were installed at the ventilator - extractor damper where draft is induced to facilitate the ascension of gases within the tower, as seen in figure 7a. The samples were removed from the ventilation vents at 15-day programmed intervals until completing a total of six (6) samples for the study of corrosion advance. Figure 7b shows the ventilator extractor where the samples were placed, allowing them to be attacked by the vapors expelled through this place.

The samples were metallographically analyzed through the Leyca Q'Metals' image analyzer. Images were taken using an optical microscope. Through this procedure we were able to establish which of the welding processes yielded the highest deterioration due to corrosion. Then, we obtained Scanning Electron Microscopy (SEM) images to analyze surface morphology.

To obtain optical microscopy images, the samples were attacked with a solution that included: 5 cm3 of nitric acid, 3 cm3 hydrochloric acid, and 2 cm3 of hydrofluoric acid mixed in 20 cm3 of water. The samples were kept submerged for 4 seconds each.

(a) (b)

Figure 7. Photos of the attack-sites of samples: a) Ventilator extractor where samples were placed, b) Ventilator damp where samples were anchored.

6. Results and analysis

Optical microscopy analyses reveal that in samples welded with the GMAW process, a segregation phenomenon occurred on the welt – as shown in figures 8a and 8b. It was also found that in the segregated zones, corrosion was quite high, as observed in figures 9a, 9b, 10a, and 10b.

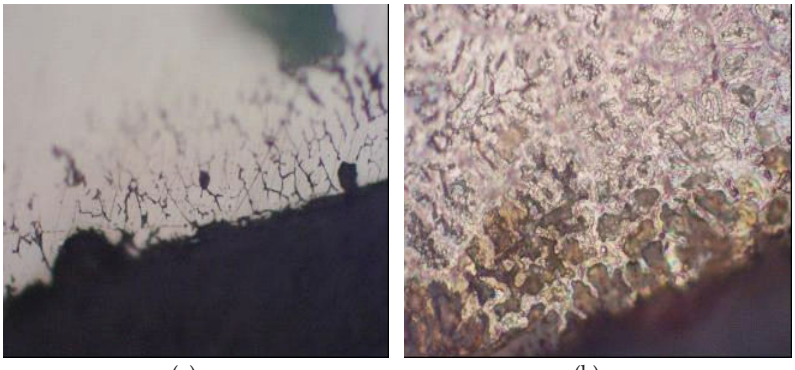

(a) (b)

Figure 8. Optical Microscopy Images of samples with GMAW welding process; removed after 1.5 months: a) Non-attacked sample – X50 welding welt, b) attacked sample, X500 fused zone.

http://dx.doi.org/10.5772/52986

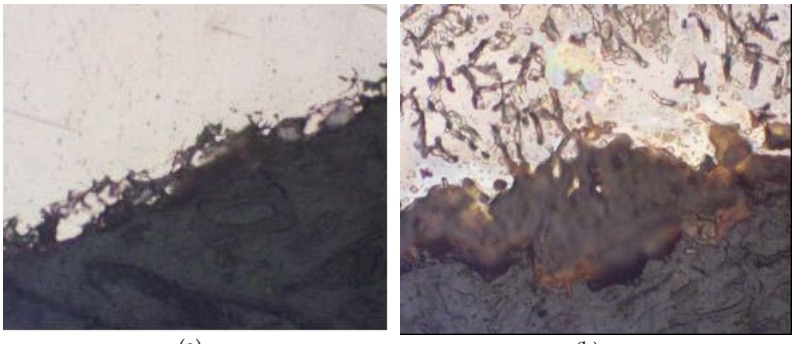

Figure 9. Optical Microscopy Images of samples with SMAW welding process; removed after 1.5 months: a) Non-attacked sample – X500 welding welt, b) attacked sample, X500 fused zone.

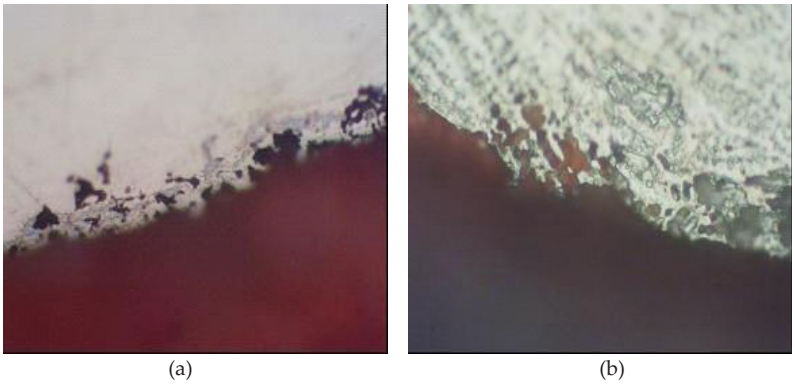

Figure 10. Optical Microscopy Images of samples with GTAW welding process; removed after 1.5 months: a) Non-attacked sample – X500 welding welt, b) Zone defused and attacked with acid.

In order to analyze the segregated zone and establish this zone's morphology and composition, a scanning optical microscopy and EDX microprobe were used, carrying out particular microanalysis on the segregated zone according to figures 11a, 11b, 12a, and 12b and on non-segregated zones as evidenced in figures 13a and 13b. Through the microprobe analysis we found the possible existence of chromium carbides formation in these zones, especially in the GMAW process, which would explain why corrosion was originated on segregated zones where carbon migration to the zone with the greatest segregation took place, with which an increased concentration of carbon can be obtained, increasing the possibility of carbide formation and decreasing resistance to corrosion. In addition, given the chemical dissimilarity between the segregated and non-segregated zones, a galvanic pair is generated, which increases the phenomenon.

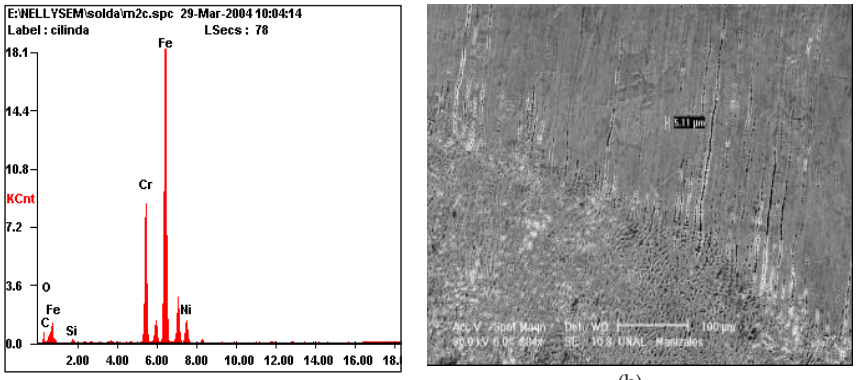

Figure 11. a) EDX Spectrum, b) SEM image of segregated zone of samples with GTAW processes; removed after 1.5 months.

Once optical microscopy and SEM images of samples welded with the GMAW process were compared and analyzed, it was observed that these were the most affected by inter-granular corrosion, as seen in figures 8, 12, and 13. In the segregated zones within the welt, samples treated with SMAW processes (figure 9) and GTAW processes (figures 10 and 11) corrosion advance was not as significant.

The comparative analysis among the samples revealed, in time, corrosion increase, probably due to the fact that corrosion advances through the segregated zone and presenting a phenomenon of corrosion through chipping [22, 24, and 29], which began as intergranular type corrosion.

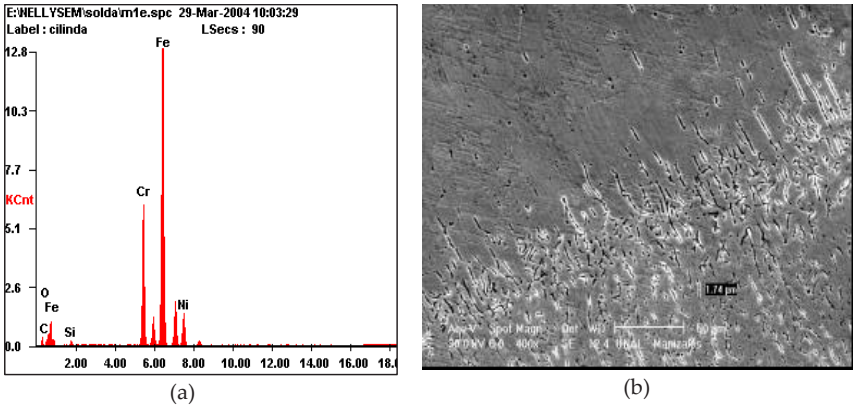

Figure 12. a) EDX Spectrum, b) SEM image of segregated zone of samples with GMAW processes; removed after 1.5 months.

http://dx.doi.org/10.5772/52986

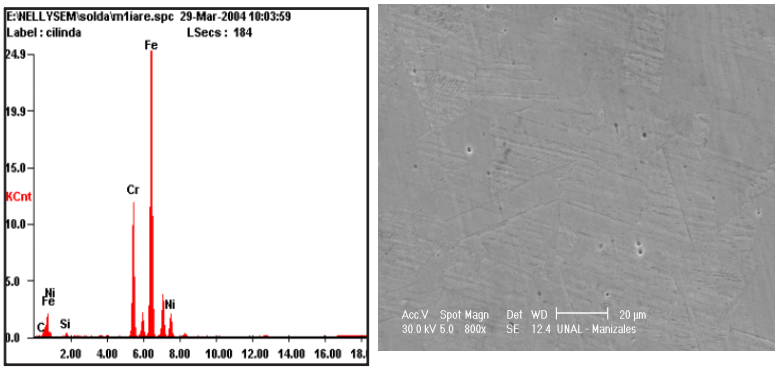

(a) (b)

Figure 13. a) EDX Spectrum, b) SEM image of non-segregated zone of samples with GMAW processes; removed after 1.5 months.

The literature mentions that intergranular corrosion is generated in the thermally affected zone [29], in this research the problem of inter-granular corrosion occurred in the solder welt, especially with the GMAW process, probably due to the segregation phenomenon [11] that could have caused the precipitation of M7C3 or M23C6 chromium carbides [30], given the chemical composition registered in the zones observed in the EDX Spectra.

7. Experimental details wear and corrosion behavior of W/WC bilayers deposited by magnetron sputtering

In this work, bilayers of tungsten W and tungsten carbide WC by r.f. magnetron sputtering reactive technique were deposited on AISI 420 stainless steel of 16 mm diameter and 3.8 mm thick substrates. The used parameters were power density 0.045 W/mm2; working pressure 5 mtorr; gas mixture with 40%, 60% and 80% CH4 balanced with Argon; W-Target 99.99% purity, 100 mm diameter; 70 V bias voltage and 70 mm distance between Target and substrate.

Previous works [38], where the microstructure and composition of WC coatings, as methane content in the gas mixture Ar/CH4 were investigated, showed that when the methane content was less than 10% the structure was principally W2C hexagonal phase [39].For methane contents between 17-23% [40] a structure composed by the cubic WC1-x with a preferred (111) orientation imbibed in an amorphous carbon matrix. A hardness level of about 25 GPa was attained and approximately 40% W in the coating. Above this methane tenors the amorphous carbon phase becomes more evident, this phase has a lower friction coefficient and it is also auto lubricant, and wear resistance is increased.

The steel was characterized by chemical and metallographic analysis; the specimens were heat treated by quenching from 1000 °C into oil and tempered at 200 °C for 1 hour; Rockwell

C hardness and roughness with 0.8 mm sensor shifting tests were carried out. The measured Rockwell C hardness was the mean of 5 tests given the following results, 14 RC before the heat treatment and 27 RC as quenching and tempered.

Before growing the bilayers a thin Ti film was grown to better the adherence between bilayers and steel. The corrosion behavior of the coatings was analyzed by using the potentiostatic test method. To determine the wear resistance the pin on disk test was used with the following parameters:

Parameters	Values
Pin initial weight (g)	0.8813
Uncoated probe initial weight (g)	5.8155
Pin diameter (mm)	6
Applied load (N)	2
Displacement (m)	2500
Angular speed (rpm)	100
Trace wear radii (mm)	3.5

Table 1. Experimental parameters setting used with the pin on disk test.

8. Results and discussion

8.1. Heat treatment of steel substrates

The AISI 420 steel micrographs, before and after the heat treatment HT are presented in figure 14. In figure 14a an austenitic phase is present while in figure 14b after heat treatment, it could be observed a martensitic phase with small carbides. These structures are in accordance with the SAE metals handbook.

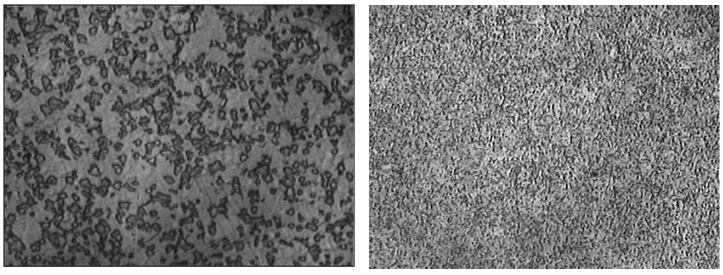

(a) (b)

Figure 14. AISI 420 steel micrographs a) without heat treatment HT and b) after heat treatment HT.

http://dx.doi.org/10.5772/52986

The Rockwell C hardness here reported is the mean of 5 tests given the following results, 14 RC before the heat treatment and 27 RC as quenching and tempered.

8.2. Corrosion behavior of coating system

In figure 15 the polarization curves are presented. The Taffel curves are registered under static conditions and correspond to probes with and without coatings. The corresponding ones to films grown with 60% CH4 and 80% CH4 showed a shifting to lesser current densities indicating a higher corrosion resistant as compared with that of the probe without coating, and the one corresponding to 40% CH4.

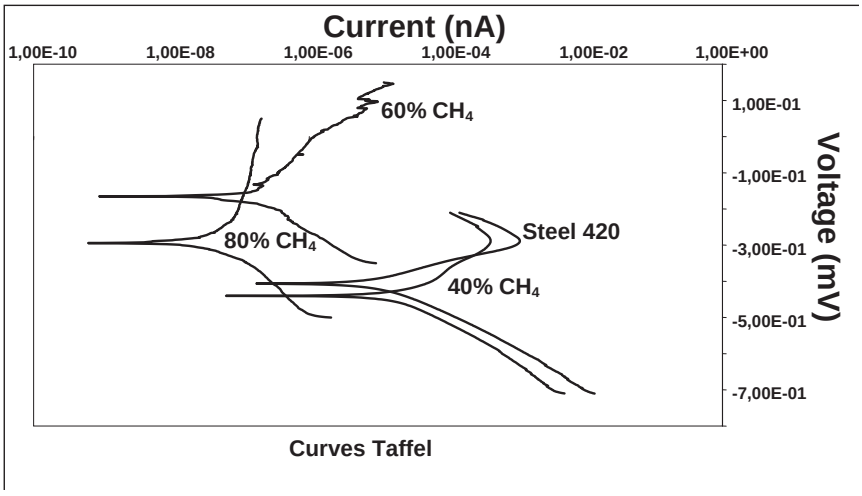

Figure 15. Polarization Curves of the different steel substrates without and with bilayers.

These two last curves behave similarly. It is possible that the low coating adherence were a consequence of the peeling of the coating associated with an anodic current peak presence as can be seen in figure 15, further visual analysis allows supposing that the presence of located corrosion due perhaps to weak mechanical stability of the coating, dissolves the substrate under the coating with an inevitable peeling. The 60% and 80% CH4 curves exhibit a tape increase of the anodic curve and corrosion intensity decrease indicating that the system is under anodic control. Figure 16 shows an AISI 420 steel without coating. A homogeneous attack over the entire surface is observed.

Figure 16. AISI 420 steel micrograph attacked by electrochemically corrosion.

In Figure 17 the surfaces of the bilayers grown at 40% 60% y 80% CH4 after the corrosion test are presented. The one at 40% CH4 were peeled, while the other two presented a kind of pitting corrosion.

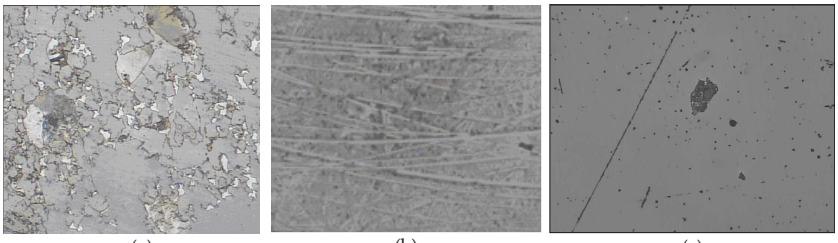

Figure 17. Attacked electrochemical corrosion surface bilayer micrographs a) 40% CH4, b) 60% CH4 and c) 80% CH4.

The inhibition of the cathodic and anodic processes can be obtained from the data in table 2.

Substrate	Ecorr (mV)	Icorr (A)	Corrosion Rate (mpy)
AISI 420 steel	-407,0	10x10-6	4,587
40% CH4	-440,0	29x10-6	13,25
60% CH4	-293,0	127x10-9	0.05833
80% CH4	-165,0	281x10-9	0.1286

Table 2. Data from the electrochemical corrosion test on probes without and with coatings.

http://dx.doi.org/10.5772/52986

The corrosion speed expressed as corrosion current Icur. was calculated by using the extrapolation Taffel method. The 40% CH4, according data in table 2 shows a corrosion potential more negative as compared with the other two, indicating a system more active and thus lesser corrosion resistance.

The roughness measured on the plain steel was 0.02 μm, whilst that of the W/WC bilayers was 0.24 μm, 0.26 μm and 0.29 μm for 40% CH4, 60% CH4 and 80% CH4, respectively.

9. Tribological properties

The films were undergone to the wear test using the pin on disk technique. Figure 18 shows the curves friction coefficient versus sliding distance. These curves correspond to the coatings W/WC grown with 40, 60 and 80 % of CH4, respectively. As it is evident they exhibit three important and well defined regions. The first zone between 0 m and 500 m, of the displacement when a sudden increase in the friction coefficient is present, due to the initial contact between the pin and the probe, the intermediate region between 500 m and 1100 m of the displacement a diminution is present due to a more flat surface, and finally in region three when the coefficient is stable.

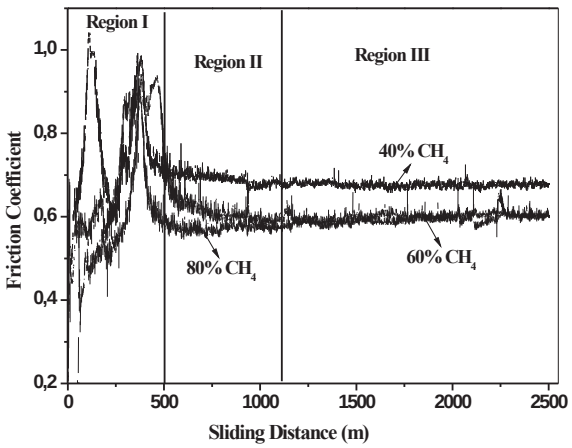

Figure 18. Friction coefficient of hard coatings W/WC grown with different CH4 on to steel AISI 420 as a function of sliding distance.

The graph reveals a slight increase in the friction coefficient that is associated with a process of micro- welding that are formed and destroyed as the pin slips on the probe and as the

material wear out allowing the formation of new surfaces. These new surfaces have a tribological behavior different from that of the original surface.

The test showed that the behavior of the AISI 420 steel without a coating and the one belonging to the film grown with 40% of CH4, was similar, the third region show a stabilized friction coefficient of 0.679. The curve corresponding to the bilayer behavior W/WC grown with 40% CH4, shows in the second and third region a higher friction coefficient value as compared with the films grown with 60 y 80% CH4.

Figure 18 shows the curve corresponding to the behavior of the bilayer W/WC at 60% CH4. The friction coefficient stabilizes at 0.602, while the curve corresponding to the bilayer grown with 80% CH4 showed a similar behavior to which of the bilayer with 60% CH4, but its friction coefficient stabilized at 0.585.

The test pin-on-disk traces were analyzed by using an image analyzer. In figure 19 the observed trace on the AISI 420 steel is almost homogeneous, but wear is too severe.

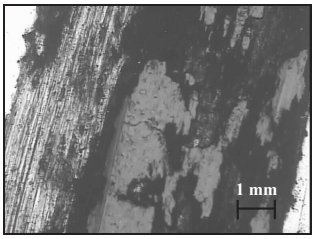

Figure 19. Photomicrograph showing the wear patterns AISI 420 steel.

The micrographs of figure 20 exhibit the wear surfaces of the bilayers. Figure 20a corresponds to W/WC 40% CH4 this bilayer shows an excessive wear, in some places the peeling of the film was observed.

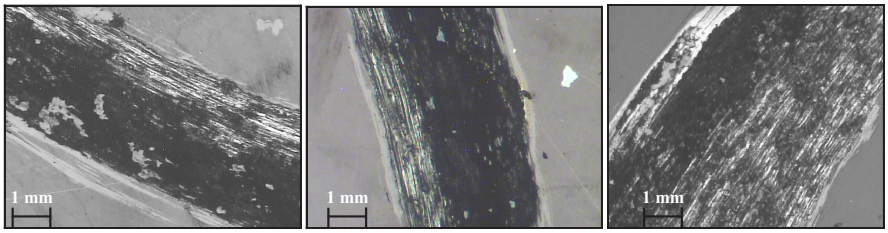

Figure 20. Trace micrographs on AISI 420 coated steel with W/WC. a) 40% CH4, b) 60% CH4 and c) 80% CH4 bilayers

Figure 20b and 20c corresponding to 60% and 80% of CH4 respectively, can be observed a homogeneous wear without the peeling of the films.

http://dx.doi.org/10.5772/52986

The above results showed that the bilayers grown with 80% CH4 present lower friction coefficient and higher wear resistant, when compared with the bilayers grown with 40% and 60% CH4, This allows concluding that as the methane percentage increases in the gas mixture a better film adhesion to substrate is presented. Therefore it's sure that the structure was principally composed by the cubic WC1-x phase with a preferred (111) orientation imbibed in an amorphous carbon matrix.

Sample	Initial Weight (mg)	Loss Weight (mg)	Friction Coefficient
AISI 420 Steel	4.3345	1.5	0.679
40% CH4	5.2351	0.98	0.679
60% CH4	5.1812	0.12	0.602
80% CH4	4.9566	0.10	0.585

Table 3. Data about the material lost and friction coefficient during the pin on disk test.

The wear of the bilayers is summarized in table 3. The higher value corresponds to that one grown at 40% CH4, while the one of those with 60% and 80% CH4, have lower values.

10. Conclusions

TiC monolayers and Ti/TiN/TIC/TiCN multilayers were grown through the pulsed-laser technique on AISI 4340 steel. It was determined that the adhesion of the films is quite acceptable. When the tension test was applied there was no detachment of the substrate on the monolayers or the multilayers. For AFM, it was found that the multilayers presented finer grain size, as well as lower roughness than the monolayers. The wear tests revealed that the multilayers showed better resistance than the TiC monolayers. In corrosion tests, the multilayers presented a lower mass loss and the film was not attacked by corrosion in its totality, keeping in mind that the medium was quite aggressive. This indicates that in engineering applications, where corrosive environments are present in the workplace, the recommendation is to use multilayered coatings on AISI 4340 steel, or any other with similar chemical properties.

In both optical microscopy images and SEM images we observed that samples treated with the GMAW welding process were most affected by intergranular corrosion, in segregated zones within the welt; whereas in samples welded with SMAW and GTAW processes the corrosion advance was not as significant. Perhaps the cause for the corrosion phenomenon described is due to segregation levels present in the solder welts, which generated – according to the results – greater presence of carbon in the segregated zones and, additionally, a galvanic pair is registered between the segregated and non-segregated zones; thus, accelerating the corrosion phenomenon.

The W/WC bilayers were grown on AISI 420 stainless steel by using the magnetron reactive sputtering technique. The corrosion tests have shown that the steels coated with 60% and

80% CH4 in the gas mixture exhibit high corrosion resistance. The wear tests established the steel coated with W/WC bilayers with 60% and 80% CH4, in the gas mixture were more wear resistance than the others. These results will be validate on the next time at industrial scale through the coating on cutting tools at the pilot magnetron sputtering facilities of CDT ASTIN and their corresponding cutting tests.

Acknowlegment

This work was financed by the office of Research and Technological Development at the *Universidad Autónoma de Occidente*, Cali Colombia, and supported by COLCIENCIAS under the program Excellence Center for Novel Materials, contract No. 0043-2005. The authors wish to thank the Tribologic and Surfaces Laboratory at the *Universidad Nacional*, Medellín Colombia, directed by Dr. Alejandro Toro.

The authors thank Ingenio Providencia – the sugar mill – for facilitating the field samples at their facilities. Characterization of samples was done in the Materials lab at UAO and at the Plasma lab of Universidad Nacional de Colombia, Manizales.

This work was supported by COLCIENCIAS under the program Excellence Center for Novel Materials, CENM contract No. 0043-2005. The growth of the bilayers was carried out at pilot facilities of SENA-ASTIN and the films characterization at the Marco Fidel Suarez School.

Author details

N. A. de Sánchez[1,2,5*], H. E. Jaramillo[1,2,5], H. Riascos[3,5], G. Terán[1], C. Tovar[1,2], G. Bejarano G.[5,6,7], B. E. Villamil[1], J. Portocarrero[1,3], G. Zambrano[4,5] and P. Prieto[4,5]

*Address all correspondence to: nalba@uao.edu.co

1 Science and Engineering of Materials Group, Colombia

2 Mechanical Engineering Program, Universidad Autónoma de Occidente, Cali, Colombia

3 Department of Physics, Universidad Tecnológica de Pereira, Pereira, Colombia

4 Thin Film Group, Department of Physics, Universidad del Valle, Cali, Colombia

5 Excellence Center for Novel Materials, Universidad del Valle, Cali, Colombia

6 Group for Engineering and Materials Development, CDT ASTIN-SENA, Colombia

7 Cali-Colombia, Centre for Research, Innovation and Development of Materials CIDEMAT, Universidad de Antioquia, Medellín,, Colombia

References

[1] A. Y. Liu and M. Cohen, Physics Rev. B 41, 10727 (1990)

[2] D. Sanders, A. Anders, Surf. Coat. Technol, 133 (2000) 78

[3] S. Veprek, J. Vac. Sci. Technolo. A 17, (199) 2401

[4] Y. Kusano, J.E. Evetts, R.E. Somekh, and I.M. Hutchings, Thin Solid Films Elsevier 56, (1998), 1272

[5] Y. Kusano, Z. H. Barber, J. E. Evetts and I. M. Hutchings, Surface and Coatings Technology 124 (2000) 104

[6] M. Show Wong, A. Lefkow, and W. Sproul, Group Program Prospectus BIRL Northwestern University Illinois 60201 (1999)

[7] M. Teter, MRS Bulletin 22, January (1998)

[8] A. Toro, A. Sinatora, D.K. Tanaka, A.P. Tschiptschin, Wear 251 (2001) 1257

[9] Diana López, Carlos Sánchez, Alejandro Toro, Wear 258 (2005) 684

[10] U. Helmersson, S. Todorava, S. A. Barnett, J. Sundgren, J. Appl. Phys. 62 (1887) 481

[11] P. B. Mirkarimi, L. Hultman, S.A. Barnett, Appl. Phys. Lett. 57 (1990) 2654

[12] H. Ljungcrantz, C. Engström, L. Hultman, M. Olsson, X. Chu, M. S. Wong, W. D. Spoul, J. Vac. Sci Technol. A16 (1998) 3104

[13] K. K. Shih, D. B. Dove, Appl. Phys. Lett. 61 (1992) 654

[14] J.P. Tu, L.P. Zhu, H.X. Zhao, Surf. Coat. Technol., 122 (1999) 176

[15] Wilson, S. and Alpas, A.T., Wear, 245, (2000) 229

[16] X. Wang. A. Kolitsch, W. Möller, Appl. Phys Lett. 71 (1997) 1951

[17] K. L. Mittal, Adhesion measurement of films and coatings, Utrecht (1995)

[18] H.M. Clark, K.K. Wong, Wear 186 (1995) 454

[19] Bhowmick S., Kale A. N., Jayaram V., Biswas S. K., Thin Solid Films, 436 (2003) 250.

[20] Smith, William F. Fundamentals of Science and Engineering of Materials. 3rd edition. McGraw Hill, Interamericana. pp. 595 – 636; 1998.

[21] http://www.corrosiondoctors.org/principles/theory.htm. Último acceso 20 de Mayo de 2004.

[22] Botia F., J. S. Ingeniería de Corrosión. Instituto Nacional del Acero. Bogotá, D. E. 12/1985.

[23] http://ionis.com.ar/agua/corrosion.htm Último acceso 27 de Marzo de 2004.

[24] Roberge, Pierre R. Handbook of Corrosion Engineering. Editorial McGraw Hill; 2000.

[25] Reina Gómez, Manuel. Soldadura de los Aceros Aplicaciones, Second Edition. Graficas Lormo; 1988.

[26] Smith, William F. Fundamentals of Science and Engineering of Materials. 3rd edition. McGraw Hill, Interamericana; 2000.

[27] Document by Ingenio Providencia Titled: Sulfitación del jugo; 2001.

[28] Kuo, Sindo. Welding Metallurgy, Second Edition. Wiley-Interscience. A John Wiley & Sons, Inc., Publication. 2003

[29] Otero Huerta, Enrique. Corrosión y Degradación de Materiales; Editorial Síntesis S.A.; 1997.

[30] Easterling, Kenneth. Introduction to the Physical Metallurgy of Welding. First Published. Editorial Dutterworths; 1983.

[31] Okazaki. Y. Ito, K. Kyo, T. Tateishi, Mat. Sci. Eng. A213 (1996) 138.

[32] J.A. Sue, T.P. Chang, Surf. Coat. Technol. 76-77 (1995) 61.

[33] L.J. Yang, Determination of the wear coefficient of tungsten carbide by a turning operation, Wear 250 (2001) 366–375.

[34] J.A. Sue, T.P. Chang, Surf. Coat. Technol. 76-77 (1995) 61.

[35] H. Dimigen, H. Hübsch, Carbon containing sliding layer, USPatent 4 525 417 (1985).

[36] H. Dimigen, H. Hübsch, R. Memming, Appl. Phys. Lett. 50 (1987) 1056.

[37] E.A. Almond, M.G. Gee, Results from a U.K. inter-laboratory Project on dry sliding wear, Wear 120 (1987) 101–116.

[38] Y. Liu, M. Gubisch, W. Hild, M. Scherge, L. Spiess, Ch. Knedlik, J.A. Schaefer, Nanoscale multilayer WC/C coatings developed for nanopositioning part II: friction and wear, Thin Solid Films 488 (2005) 40-148.

[39] C. Rincón, G. Zambrano, P. Prieto, Propiedades mecánicas y tribológicas de monocapas de W-C, DLC y multicapas de WC/DLC, Revista Colombiana de Física, vol. 35, No. 1 (2003).

[40] A. Voevodin, J.P. O`Neill, J.S. Zabinski, tribological performance and tribochemistry of nanocrystalline WC/ DLC composites, Thin Solid Films vol. 342, Issue 1-2 (1999) 194-200.